SSRG International Journal of Geo-informatics and Geological Science
ISSN: 2393 – 9206 /doi:10.14445/23939206/IJGGS-V8I2P108

Volume 8 Issue 2, 89-105, May-Aug, 2021

Original Article

Comprehensive Model on Major Litho-Units in Central Part of Chitradurga Schist Belt of Dharwar Craton, Karnataka, India for Indian Spectral Library Generation

Manjunatha M.C[1] and Basavarajappa H.T[2]

[1]*Department of Civil Engineering, Maharaja Institute of Technology, Thandavapura, Mysuru-571302, India*
[2]*Department of Studies in Earth Science, CAS in Precambrian Geology, University of Mysore, Mysuru-570006, India*

Received Date: 08 July 2021
Revised Date: 10 August 2021
Accepted Date: 23 August 2021

Abstract *- Precambrian basement rocks of Chitradurga Schist Belt (CSB) in Dharwar Craton comprises of enormous ore deposits, lithological contacts and mineralized zones. Spectral signatures of a mineral/ rock/ ore have opened a new vista in their scientific exploration and systematic mapping. In present study, 14 random samples of iron, manganese, limestone, komatiite, gneiss, fuchsite quartzite, conglomerate, biotite-granite, metagabbro, copper ore, dolerite, auriferous quartz, quartz vein and actinolite-tremolite schist are collected from central part of the Chitradurga Schist Belt of Dharwar Craton. These major rocks and minerals are studied as thin section under microscope, ICP analysis and ASD FieldSpec[3] Spectro-radiometer to construct a model to map such resources successfully. This study synthesized the relationship of spectral absorption features of the rock/ mineral samples with the major and minor mineral constituents and compositions. Comprehensive model is a theoretical constructed design in the present study to seek more information under one platform to construct a spectral library for the selected samples along with their modified geological succession. This model also refers the spectral signatures of minerals, the rocks available in the USGS, JPL and JHU spectral library, in the vision to develop a spectral library of minerals of India.*

Keywords: *Petrography, Geochemistry, Spectral Signatures, CSB, Comprehensive model.*

I. INTRODUCTION

Chitradurga Schist Belt is represented by a thick pile of volcanic flows and sediments, iron and manganese ore formations occur in both off shore volcano-sedimentary sequence as well as in plat formal sedimentary sequence (Swaminath and Ramakrishnan, 1981; DID, 2006). Prominent bands of ore formations, mineralized zones are exposed forming a continuous chain of hills with local concentration of different lithological contacts occurs all along Block-A (Figure 2) (Swaminath and Ramakrishnan, 1981; Manjunatha et al, 2017a). The important ore deposits are near Vajra and Kudrekanna, Lakkihalli, kenkere, Bheema Samudra, Bhahaddur Ghatta, Hosahatty and Madakaripura. The regional trends of the bands are NNW-SSE with steep easterly dip (Swaminath and Ramakrishnan, 1981). The trends of the foliations are more or less parallel to banding. The ore formations show three types of banding viz., macro-band, meso-band and micro-band along with pene-contemporaneous deformation structures (Swaminath and Ramakrishnan, 1981) with intense deformation and metamorphism.

Spectral reflectance is an optical property of materials that describes the light in a continuous electromagnetic spectrum interacts with the material (Ali M. Qaid et al., 2009). The amount of light reflected at any given wavelength is a function of the elemental content and molecular structure of the materials and measurement of reflected light across the Visible and Near-InfraRed wavelengths (Hoover et al., 1993). The spectral signatures of rocks rely on the spectra of the constituent minerals and their textural properties like grain size, packing and intermixture (Gupta, 2003). Reflectance spectroscopy of rocks and minerals can give useful diagnostic information on their elemental and mineralogical composition (Hunt, 1977).

Ramachandran et al., (1982) explained a low cost portable spectro-radiometer made in 1983 with spectral range from 0.5 to 1.0 microns has been built at ISRO Satellite Centre, Bangalore (Thutupalli et al., 1981) which found useful for in-situ spectral reflectance studies for discrimination between rock types from Chitradurga area of Karnataka. He had discussed that ferruginous and

manganiferous cherts are discriminable by their quantum of reflectance; while fuchsite quartzite and barites shows similar spectra (prominent peaks) in green wavelength due to its green chrome bearing mica fuchsite. Absorption bands around 0.60, 0.84, 0.90 and 0.96 microns are observed in milky quartz, whose significance is not understood.

Study of hyperspectral signature of minerals using "laboratory grade" spectroscopic principles (Clark et al., 1990) is additionally vital for identification and mapping of surface mineralogy and rock types which are carried by several geologists (Basavarajappa et al, 2017a). Laboratory spectral-radiometer instrument has their own light source for illumination of the specimen and has very high spectral resolution and measuring reflectance percentages of samples from 400 to 2500 nm (Lipton, 1997; Basavarajappa et al, 2016). The troughs within the obtained spectra are the absorption features representing the diagnostic characters of a unique mineral will be understood by determining the dimension and depth of the spectra (Lipton, 1997; Basavarajappa et al, 2017a).

II. METHODOLOGY

In this study, random samples of major rocks, minerals and ores of CSB have been collected during extensive field visits for laboratory study (Manjunatha, 2017b) (Fig.1; Table.1). Garmin eTrex-10 of 3m error handheld GPS is used to record the co-ordinates of each samples collected during field survey (Manjunatha and Basavarajappa, 2020). The samples are studied for petrographic characters using a microscope by preparation of microscopic thin sections and were analyzed for major chemical elements analyses using an ICP (Inductively Coupled Plasma Spectrometer) instrument (Manjunatha, 2017b; Basavarajappa et al, 2017b). Hyperspectral measurements of field samples are carried out using a spectro-radiometer instrument, FieldSpec^3 (Laboratory Analytical Spectral Device), in the wavelength of 350-2500 nm at the Geological Survey of India (GSI), Bengaluru (Basavarajappa et al., 2015a; 2016). The instrument has the spectral resolution of 3 nm (at 700 nm) and 10 nm (at 1400/2100 nm) (Basavarajappa et al, 2017a; Manjunatha, 2017b). The obtained data are studied using ASD ViewSpecPro software and exported to ASCII format for further studies using Environment for Visualizing Images (ENVI) v4.6 software. The spectra are used as an end member for detailed analysis and interpretation, and compared with the spectral library such as USGS, JPL and JHU available in the ENVI software (Nisha et al., 2014; Rajendran and Sobhi Nasir., 2014).

A. Geological Settings

The earlier workers have done immense work on the study area by revealing its regional geology, geochemistry, geochronology and geophysics than other parts in Karnataka. The study area lies in the central part of the Karnataka Craton (Bruce Foote., 1882; Maclaren., 1906) which is narrow, curvilinear geosynclinal area exposes a thick pile of sediments and volcanic of the Dharwar Super group (Manjunatha, 2017b). Chitradurga group is largely made up of the sediments starting from mixed (polymictic) conglomerates of Talya village followed by limestone-dolomite, phyllite, Fe-Mn formation, sulphide iron formation, Ingaldhal volcanic and banded ferruginous chert, greywacke, chert and phyllite (Swaminath and Ramakrishnan., 1981; DID, 2006; Basavarajappa and Manjunatha, 2014).

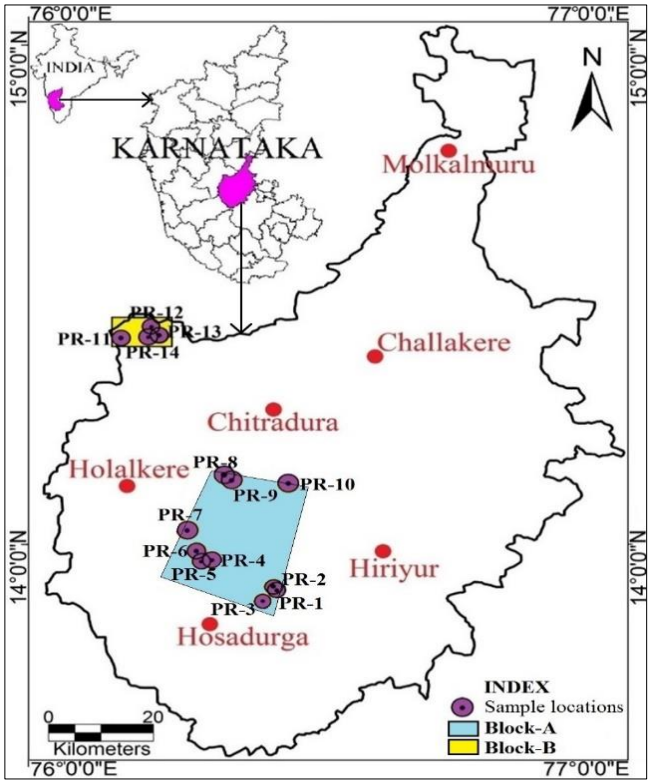

Fig.1 Location & Sample collection map of the study area

Geologically, the study area confirms Archaeans and Dharwars as basement complex represents mainly of gneisses, patches of closepet granite, granitoids and schistose formations (Swaminath and Ramakrishnan., 1981; Manjunatha and Basavarajappa, 2015b). The gneisses of the study area are "Peninsular gneiss" which is the basement rock consists of a heterogeneous mixture of several types of granitic rocks with enclosed lenses and patches of hornblendic schists (Seshadri et al., 1981). There are many parallel hill ranges are noticed as schistose rocks & general strike is N20^{0}W and S20^{0}E and dipping both in East and West directions varying from 55^0 to 85^0 (CGWB., 2013; Manjunatha and Basavarajappa, 2015c; Basavarajappa et al, 2014a; Basavarajappa and Manjunatha, 2015c). Physiographically, the study area portray undulating plains, interspersed with sporadic ranges and isolated low ranges of rocky hills (CGWB, 2013; Ravikumar et al, 2014).

Table.1 Random samples collected during field survey and its geo-location

Sample no's	Sample name	Village Location	Latitude	Longitude
PR-1	Banded Hematite Quartzite (BHQ)	Lakkihalli	$13^0$54'52''	$76^0$24'44''
PR-2	Manganeferous quartzite	Lakkihalli	$13^0$54'53''	$76^0$24'42''
PR-3	Dolo-limestone	Ramajjanahalli	$13^0$41'43''	$76^0$30'53''
PR-4	Komatiite	Kumminagatta	$13^0$57'875''	$76^0$18'126''
PR-5	Gneiss	Kumminagatta	$13^0$57'875''	$76^0$18'126''
PR-6	Fuchsite quartzite	Ghattihosahalli	$13^0$58'016''	$76^0$18'040''
PR-7	Talya Conglomerate	Talya	$14^0$0'42.35''	$76^0$17'56.58''
PR-8	Biotite granite	Pandralli	$14^0$09'149''	$76^0$20'727''
PR-9	Metagabbro	Pandralli	$14^0$09'149''	$76^0$20'727''
PR-10	Copper Ore	Ingaldhal	$14^0$10'23.74''	$76^0$26'19.84''
PR-11	Dolerite	Near Halekal band	$14^0$25'24.96''	$76^0$07'57.96''
PR-12	Auriferous quartzite (Gold bearing)	Hosahatti	$14^0$26'5.01''	$76^0$8'58.63''
PR-13	Quartz vein (Lepidolite bearing)	Hosahatti	$14^0$26.6'39''	$76^0$09'6.02''
PR-14	Actinolite-Tremolite Schist	Hosahatti	$14^0$26'1.33''	$76^0$09'1.43''

Note: PR: Precambrian rocks; Sample location map (Fig.1 & 2)

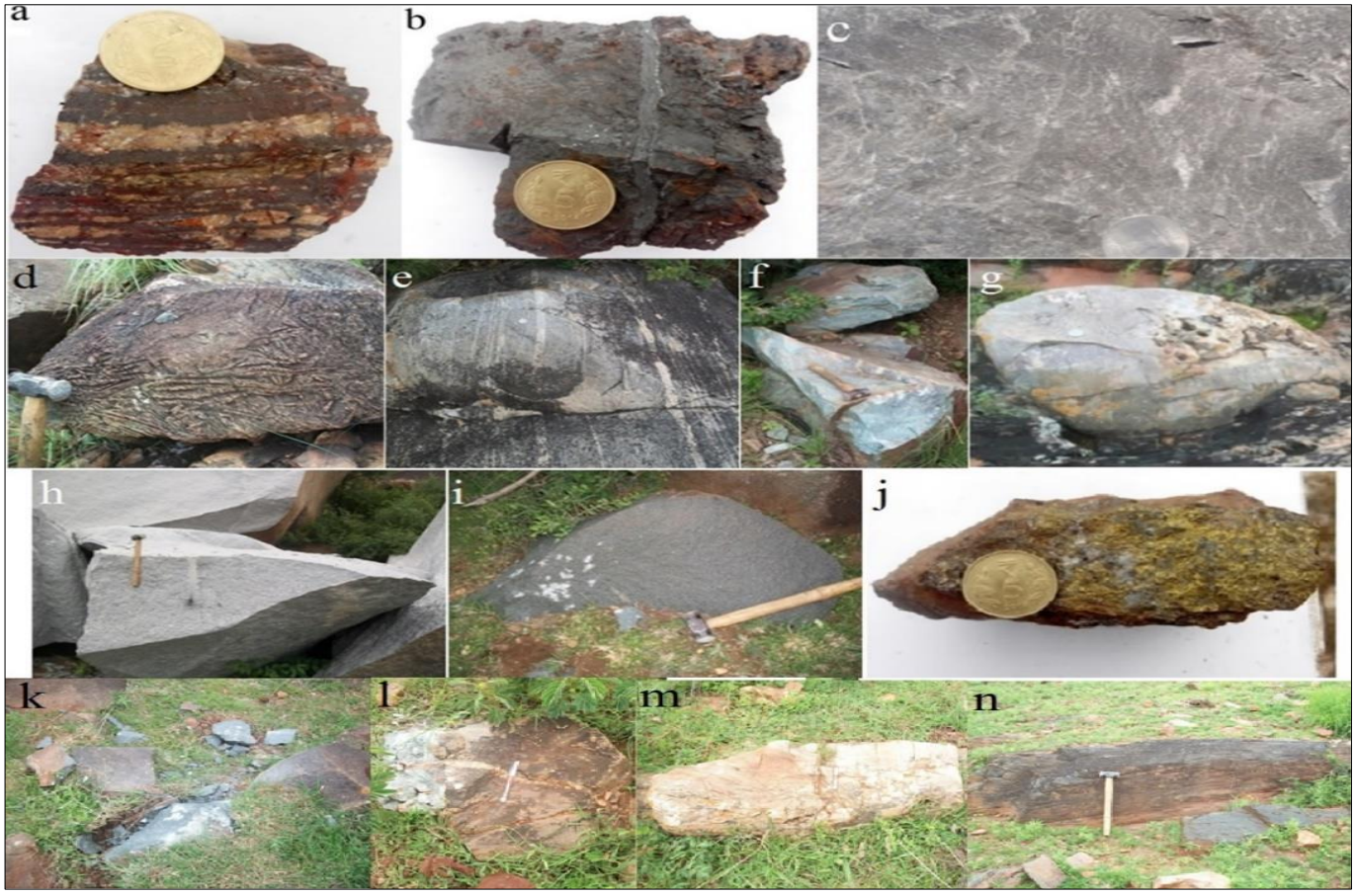

Fig.2 a. Banded Hematite quartzite (**PR-1**); b. Manganiferous quartzite (**PR-2**); c. Dolo-limestone (**PR-3**); d. Komatiite (**PR-4**); e. Gneiss (**PR-5**); f. Fuchsite quartzite (**PR-6**); g. Talya conglomerate (**PR-7**); h. Biotite granite **PR-8**); i. Metagabbro (**PR-9**); j. Copper ore (**PR-10**); k. Dolerite (**PR-11**); l. Auriferous quartz (**PR-12**); m. Quartz vein (**PR-13**); n. Actinolite-tremolite schist (**PR-14**)

a) Regional traverse along Block-A: Lakkihalli area is noticed under Lakkihalli state forest of Hosadurga taluk with general elevation of 743 to 779 m above MSL (Manjunatha et al, 2015a; 2018) (Fig.3). BHQ's are well exposed along N-S strike shows banded in nature, fine grained, grayish in color. The banding is due to silicate and iron rich oxide (Fig.2a). The iron ore deposit consist mostly limonite, goethite and hematite minerals (Basavarajappa et al, 2015a; Manjunatha and Basavarajappa, 2021). The formations are rich in supergene enriched hematitic ore majorly derived from the secondary enrichment of Banded Iron Formation (BIF) composed mainly of banded ferruginous quartzites, conglomerates, metabasalts, phyllites and dolomites. Wherever the chert is brecciated, manganese dioxide ores fill the fractures (Fig.2b). There are several pockets both within the chert and the phyllite where the manganese ore is concentrated. Interceding of manganese ore with chert bands, co-folding of the manganese ore beds suggest that the ore is syngenetic sedimentary type, which has undergone supergene enrichment. Manganese horizon located on both sides of Iron ore band at places with same strike direction as of the Iron ore band and mixed with silica.

Limestone of Marikanave near Ramajjanahalli, consists of granite-clast. Limestone-dolomite unit is overlain by banded manganiferous chert and manganiferous phyllite (Fig.2c). In the northern parts of the dome near Ramajjanahalli, limestone directly rests on the gneiss close to this contact, the limestone not only enclose sporadic granitic pebbles but also become gritty with detrital quartz and rare feldspar grains and associated with Mn-dolomite. Limestone shows grey, compact, crystalline well bedded rock showing facies variations into manganiferous dolomites. Some of the limestone contains needle-like and stumpy crystals of amphiboles that are completely converted to calcite and cherty matter. These limestones are conglomeratic, gritty and feldspathic due to admixture with silica detritus near Ramajjanahalli village (Basavarajappa et al, 2019).

Ghattihosahalli Schist Bet (GSB) consists of volcano-sedimentary sequence includes the ultramafic komatiites, steatite, amphibolites with interlayered fuchsite quartzite, migmatitic gneiss and barite beds (Vishwanatha et al., 1977; Radhakrishna and Sreenivasaiah, 1974; Manjunatha et al, 2017a). This sequence of quartzite and barite occurs as a chain of lenticular enclaves within the peninsular gneisses (Viswanathaiah and Venkatachalapathy, 1980; Manjunatha and Basavarajappa, 2017c). Komatiites occurrence of (GSB) is spinifex textured and contains high Mg content ultramafic composition (Vishwanatha et al., 1977; Deshmuk et al., 2008) which is of volcanic/ sub-volcanic origin (Jayananda et al., 2008) formed around 3384 m.y (Prabhakar and Namratha, 2014). Lensoidal and bladed crystals of olivine showed alteration of serpentine by weathering process and randomly stacked, accentuated by thin stringers of magnetite are observed in fresh samples (Fig.2d) (Ramakrishnan et al., 2012). At few places, the komatiite is associated with quartzite signify that its occurrence is ultramafic subaqueous volcanism and chemical precipitation of eruption (Jayananda et al., 2008; Basavarajappa et al, 2017a).

Peninsular gneiss occurs extensively exposed on a small mound and low-lying hillocks, all along the western and northern parts of the Ghattihosahalli Schist belt. Gneisses in the area include grey biotite gneiss, quartzo–feldspathic veins resulting in local migmatisation (Fig.2e) (Swaminath and Ramakrishnan, 1981). The PGC exhibits complex relationship with older and younger supracrustals. Gneissic rocks are intruded by quartz at many locations & pegmatites with felsic and mafic bands are also noticed. The outcrop of fuchsite quartzite bed exposure shows peculiar greenish color due to the presence of chromite mica and quartz grains showing foliation plane (S_0) in the beds. Bedding plane S_0 shows the strike of $N50^0W$ to $S50^0E$ dipping 80^0W (Fig.2f). This outcrop shows association with amphibolite with fine grained, dark greenish to black color consisting mainly of hornblende minerals. Fuchsite quartzite layers show overturned type of fold in which both the limbs are folded more than 90^0 dipping in a single direction.

The hillocks east of Neralakatte village expose polymictic Talya conglomerate in association with greywacke siltstone and argillite (Fig.2g). The conglomerate consists of boulders and pebbles of quartzite, granitoids, and quartz vein, basic rocks, chlorite matrix. Conglomerate is intensely sheared as pebbles which are bent, twisted and torn types. Quartzite clasts are predominant and show high degree of roundness and low sphericity. The pebble size ranges from 1cm to as much as 50 cm; the matrix is made up of quartz-chlorite-actinolite and biotite. Talya conglomerate is overlain by and interbedded with chlorite schists and cross – bedded quartzite.

A part of Chitradurga schist belt is exposed of metabasalt, metagabbro and granitic sequences dominantly along Pandralli village (Fig.2h). Weathered zones are noticed along fractures and joints within the granite formations. In an outcrop, the felsic intrusive of pink granite shows light pinkish color (plagioclase), coarse grained, mainly composed of quartz, k-feldspar, plagioclase, biotite and varieties of mica. Metagabbro are encountered as dyke intrusions striking towards $N80^0E$ to $S80^0W$ dipping 75^0 towards west with a width of 52 m (Fig.2i). Huge boulders which are grey in color, medium grained with composition of quartz, feldspar and biotite marks up of Chitradurga granite representing the intrusions in metabasalt terrain.

Copper mineralization mostly occurs in quartz veins emplaced along shear zones occurring within the metavolcanics (Fig.2j). Pyrite mineralization with galena and occasional quartz veins is seen in chert bands and quartz reefs occurring within the metavolcanics. Highly oxidized, weathered parts are noticed with high concentration of pyrite and forms a massive sulphide deposits within this famous Ingaldhal mine area; while pyrite, chalcopyrite and arsenopyrite are encountered in the silisification and alteration zones. The sulphide mineralization is localized

in quartz veins occupying narrow shear zones in the metabasalts and is of polymetallic type containing copper, zinc and lead with some silver and gold values. The principal sulphide minerals are chalcopyrite, pyrrhotite, pyrite and sphalerite with minor galena (MRI, xx).

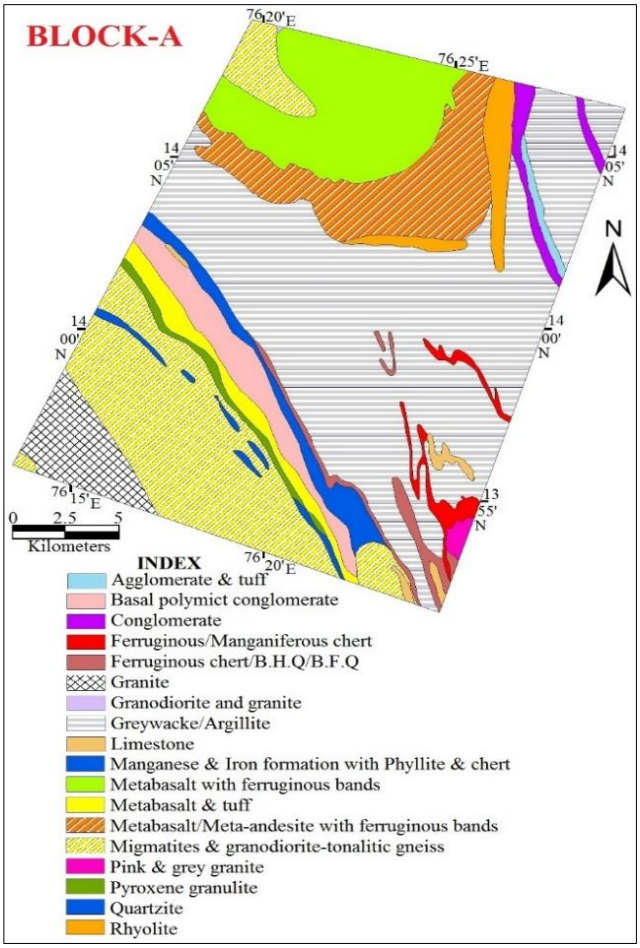

Fig.3 Lithology map of Block-A

b) Regional traverse along Block-B: The Halekal band is an outlier of Bababudan Group occurring to the north-east of Mayakonda belt between Bharamsagara and Anaji (Fig.4). It is mainly made of mafic platformal suite similar to the Mayakonda belt but at the synclinal core manganiferous sediments are noticed. The manganese formations represent the lower portions of Chitradurga Group (Basavarajappa et al, 2015b) associated with polymictic conglomerate, dolerite as dykes (Fig.2k), auriferous quartz (gold bearing) (Fig.2l), quartz viens (lepidolite bearing) (Fig.2m) and actinolite-tremolite schist (Fig.2n). These dolerites are rich with clouded feldspars which could be due to effects of regional thermal metamorphism (GSI, 2006). The Halekal belt shows amphibolite facies metamorphism at the borders and green-schist facies at the core.

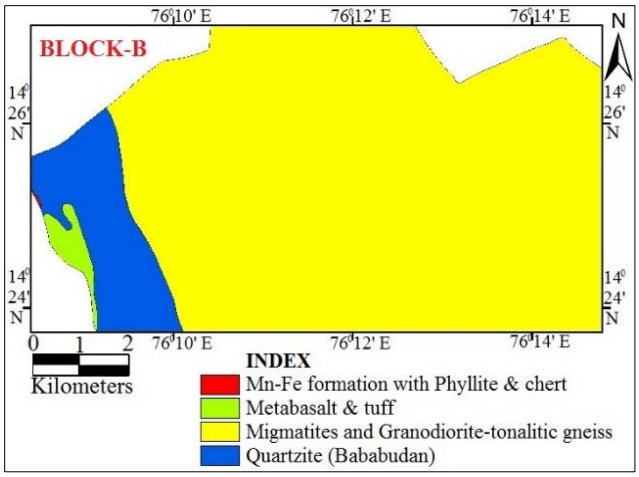

Fig.4 Lithology map of Block-B

III. RESULTS & ANALYSIS

A. Petrography and Geochemistry

In this study, fourteen representative rock samples (PR-1; PR-2, PR-3, PR-4…… PR-14) were carried carefully to the research Petrographic Laboratory at Department of Studies in Earth Science, University of Mysore, Mysuru, to make thin section for petrographic work (Table.1). A thin section of rock is cut from the sample with a diamond saw & ground optically flat and mounted on a glass slide. Then the ground parts of the samples were made smooth using progressively finer abrasive grit until the sample measure 30 µm thick. Petrographic characters of all the section were carried out using Leitz XPL-2 petro-microscope (Lawrence and Mayo).

The samples are studied for major chemical and minor trace elements at the Shiva Analytical India Pvt Ltd, Hosakote, Bengaluru. Geochemistry of 14 samples were performed by using Inductively-Coupled Mass Spectrometry (ICPMS), both quadrupole-based and high-resolution magnetic sector instruments (Manjunatha, 2017b). ICP being used mainly for trace elements, a classical triacid (HCl-HNO_3-HF) [Hydrochloric acid-Nitric acid-Hydrogen Fluoride] decomposition procedure is used; its efficiency has been improved by prolonged heating (48 hours or more) with HF in closed vessels placed in aluminum blocks at 150^0C. $HClO_4$ (perchloric acid) classically used for elimination of excess HF, has been replaced by repeated evaporation with nitric acid. Final dilution with HCl is made directly in the vessel on an electronic balance: compared to the voluming method using flasks, the procedure is simplified, a possible source of contamination is avoided, and a precise dilution ratio is computed directly on a spreadsheet. After analysis, the solution may be concentrated again for treatment on ion-exchange columns.

a) PR-1. Banded Hematite Quartzite (BHQ): BHQ shows alternate bands of Quartz (Qtz) and hematite (Fe). Quartz grains show low relief, anhedral, indistinct cleavage with alterations to sericite, goethite and exhibit characteristic

interference colors. Hematite minerals show opaque with synistral displacement and movement of fault (Fig.5). The chemical analysis of iron ore sample shows the distribution of Fe_2O_3 contents of 61.50%; SiO_2 of 25.49%; Al_2O_3 of 3.37%; MnO of 5.33%; MgO of 1.53% respectively and other oxides are given in the Table.2a. All other major oxides like TiO_2, CaO, Na_2O and K_2O are less than 0.5 wt % (Table.2a).

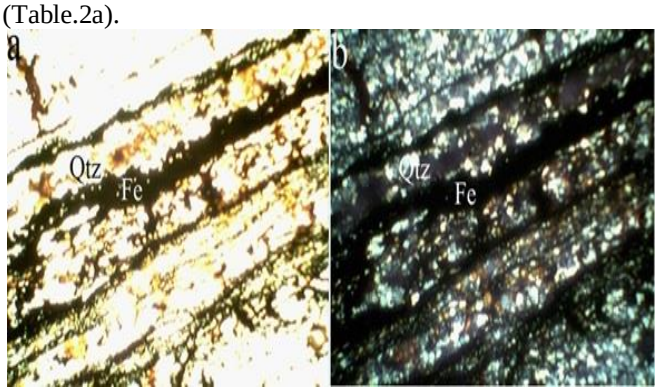

Fig.5 Photomicrograph of Alternate bands of Fe and Silica in (a) ppl, 4x and (b) xpl, 4x

b) PR-2. Manganeferous quartzite: It shows equigranular Quartz (Qtz) in association with pyrolusite, psilomelane, Manganite (Mn) and wad. Manganese is formed by the reaction of water and carbon-di-oxide. Tonalitic manganiferous quartzites are observed at certain juncture (Fig.6). The major element analysis of the rock samples showed high concentrations of MnO (34.39%), SiO_2 (42.17%), Fe_2O_3 (15.32%) and low amounts of Al_2O_3 (0.30%), TiO_2 (0.11%), K_2O (0.11%) and CaO (0.13%) (Table.2a).

Fig.6 Photomicrograph of Manganiferous quartzite in (a) ppl, 4x and (b) xpl, 4x

c) PR-3. Dolo-limestone: It's a crystalline rock of the high calcium type often showing a banded character with minor magnesium content. Under Cross Polarized Light (XPL); Calcite (Cal) shows greenish brown color and under plane polarized light shows colorless associated Quartz (Qtz) & Plagioclase (Plag). Iron oxide (Fe) is isotropic and anhedral with opaque character. Plagioclase shows alteration to Epidote (Ep) along cleavage planes (Fig.7). The major element analysis of the rock samples showed high concentrations of CaO (43.61%), H_2O as loss of ignition (42.19%) and low amount of SiO_2 (6.38%), MgO (4.94%), Fe_2O_3 (0.67%), Al_2O_3 (0.21%), Na_2O (0.05%), K_2O (0.05%) and TiO_2 (0.01%) (Table.2a).

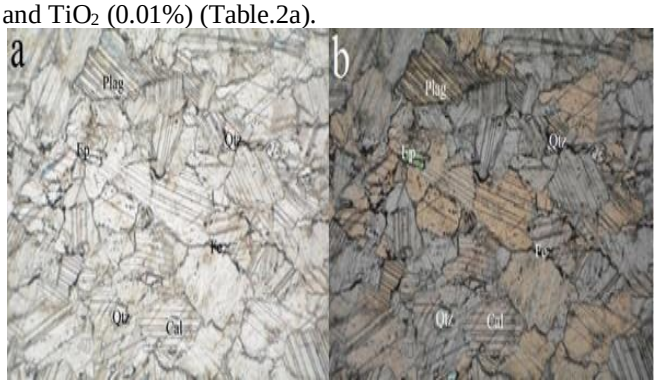

Fig.7 Photomicrograph of Dolo-limestone exhibiting well developed calcite in (a) ppl, 10x and (b) xpl, 10x

d) PR-4. Komatiites: Komatiites are mainly made up of olivine and altered serpentine minerals with streaks of magnetites (Ramakrishnan et al., 2012). The komatiite exhibited bundles of long & short olivine's, sub-parallel and cross cutting serpentines (olivine altered product) with small isolated patches of fibrous asbestos (Fig.8). The major element analysis of the rock samples showed high concentrations of SiO_2 (40.37%), MgO (32.42%) and Fe_2O_3+FeO (10.17 %) and low amounts of K_2O (0.10 %), CaO (2.37 %) and Na_2O (0.25 %) (Table.2a).

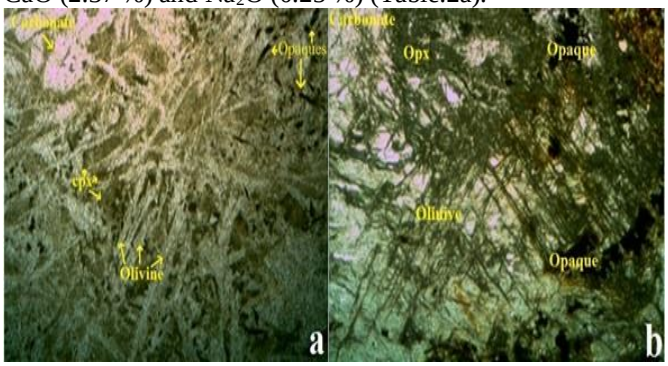

Fig.8 Photomicrograph of (a) Spinifex textured Komatiite shows (b) parallel & randomly oriented olivine blades of serpentine with minor carbonate and fine grained opaque (magnetite) minerals (ppl, 4x)

e) PR-5. Gneiss: Migmatite is consisting of Plagioclase (Plag), Chlorite (Chl), Sericite (Ser), Muscovite (Ms), Biotite (Bt) and equigranular xenoblastic grains of Quartz (Qtz). Large sericite crystals replacing plagioclase show elongation with small white micas during hydrothermal alteration (Ali M. Qaid., 2008; Rajendran et al., 2011). These vary in composition from tonolitic to trondhjemite; show porphyroblastic in nature, with subordinate perthite, biotite, epidote and muscovite. It exhibits alternating bands of feldspars + quartz rich layers with biotite grains. Plagioclase shows myrmekitic texture, while feldspar minerals are

altering to poikiloblastic (sieve) texture. Zircon alters to muscovite mica; while biotite altering to chlorite and sphene (Fig.9). Myrmekite replacing microcline and twins in the myrmekite shows quartz worms are in a plagioclase matrix. Here, k-Feldspar (Fld) was removed; while quartz and plagioclase were deposited in its place.

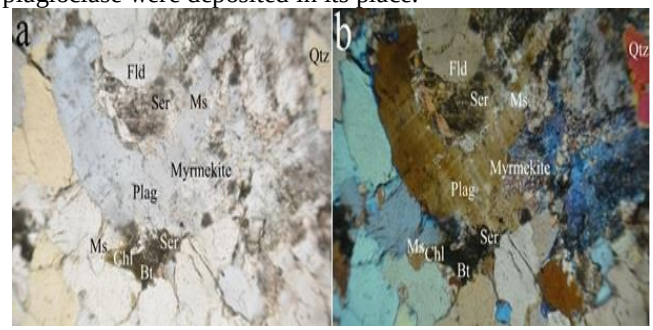

Fig.9 Photomicrograph of gneiss with myrmekitic texture in (a) ppl, 10x and (b) xpl, 10x

f) PR-6. Fuchsite quartzite: Fuchsite Mica (Fm) shows high interference color in Quartz (Qtz); while Muscovite (Ms) mica shows parallel extinction and perfect cleavage. The quartzites consist of emerald green color (chrome mica) minerals which are pleochroic in nature from yellowish green to green. Opaques are seen some has octahedral phases and some portions are not well developed, may be representing hematite (Fe) (Fig.10). The major element analysis of the rock samples showed high concentrations of SiO_2 (77.91%), Al_2O_3 (9.92%), K_2O (5.18%) and low amounts of Fe_2O_3 (1.89%), Na_2O (0.23%), MgO (0.69%) and CaO (0.43%) (Table.2a).

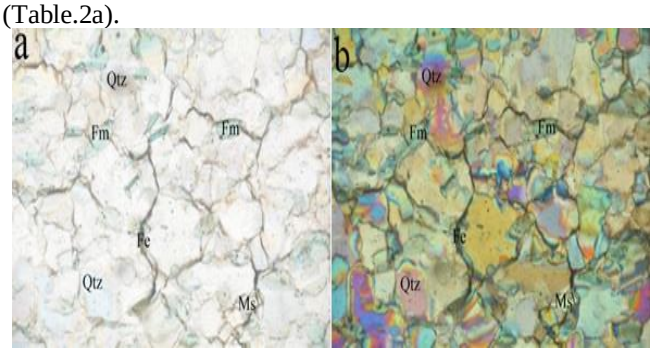

Fig.10 Photomicrograph of Fuchsite mica in association with quartzite and opaque minerals in (a) ppl, 4x and (b) xpl, 4x

g) PR-7. Talya Conglomerate: The matrix of the conglomerate is highly schistose and consists of Quartz (Qtz), Chlorite (Chl), Actionlite (Act) and Biotite (Bt). Xenoblastic grains of quartz form a fine mosaic with intergranular biotite, Muscovite (Ms), Sericite (Ser), chlorite flakes and Sphene (Sph). It shows well developed chlorite-biotite schist association with minor Magnetite (Mag); which are anhedral dark colored isotropic opaque grains. Chlorite grains exhibit subhedral with pale green to light pale green pleochroism.

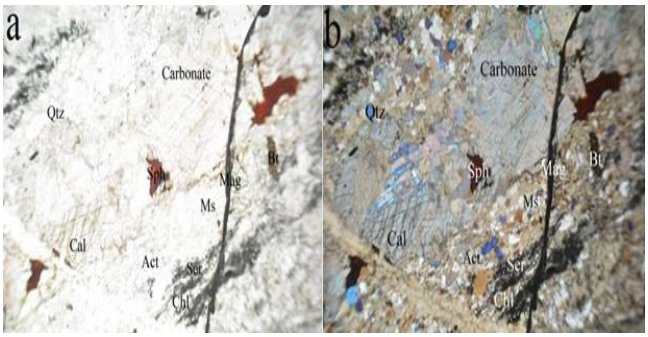

Fig.11 Photomicrograph of Talya conglomerate in (a) ppl, 4x and (b) xpl, 4x

Biotites are tabular with serrated margins, light brown in color, pleochroic from light brown to brown exhibiting straight extinction. Newly formed carbonate and calcite are observed (Fig.11). The major element analysis of the rock samples showed high concentrations of SiO_2 (65.89%), Fe_2O_3 (8.89%), Al_2O_3 (10.11%), MgO (4.13%), TiO_2 (1.23%) and low amounts of K_2O (3.29%), Na_2O (1.02%) and CaO (3.79%) (Table.2a).

h) PR-8. Biotite Granite: Phenocrysts of feldspar being arranged with their longer axis parallel to the direction of foliation with tabular and prismatic crystals. The granite is leucocratic, porphyritic and shows a mineral assemblage of Quartz (Qtz), K-Feldspar (Fld), Plagioclase (Plag), Biotite (Bt), secondary Chlorite (Chl), Muscovite (Ms) and Sericite (Ser) with accessory Sphene (Sph), apatite and zircon. Plagioclase and K-feldspar occur in two distinct phases and both show variable alteration to muscovite and sericite (Fig.12).

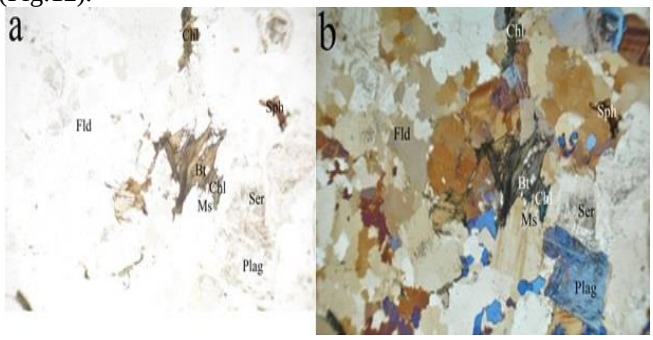

Fig.12 Photomicrograph of Biotite granite in (a) ppl, 4x and (b) xpl, 4x

i) PR-9. Metagabbro: Feldspars are converting into sericite, sub-ophitic texture of plagioclase lath type, opaques are magnetite; while chlorite and Pyroxene (Pyx) are converting into Feldspar (Fld). Silver (ag) is also present (Fig.13). The rock shows ophitic and sub-ophitic texture, wherein short stumpy prisms of augite are seen to be partially intergrown with laths of Plagioclase (Plag) some of which show feeble zoning. Sericite (Ser), Augite (Aug) and Diopside (Diop) are reacting together forming gedrite. Skeletal euhedral

magnetite is the main accessory mineral. In addition to augite, diopside and plagioclase, the rock consists of minor amounts of Hypersthene (Hyp) and titanium rich biotite. Augite is slightly brownish, tiny exsolved rods with plates of Fe-Ti oxides. The major element analysis of the rock samples showed high concentrations of SiO_2 (49.90%), Al_2O_3 (13.89%), Fe_2O_3 (10.41%), MgO (9.34%), CaO (7.70%) and low amount of K_2O (0.69%), TiO_2 (1.09%) and Na_2O (2.04%) (Table.2b).

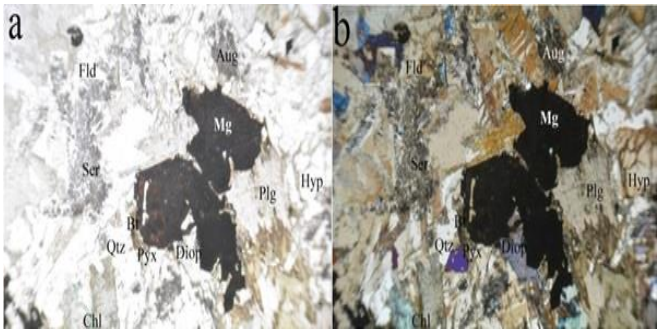

Fig.13 Photomicrograph of Metagabbro shows magnesium rich magnetite in (a) ppl, 4x and (b) xpl, 4x

j) PR-10. Ingaldhal Copper ore: Quartz grains (Qtz) are anhedral, show low relief, cleavage indistinct, alteration absent, colorless and undulose extinction. Numerous Pyrite (Pyr) crystals are observed in association with Sericite (Ser) (Fig.14). The major element analysis of the rock samples showed high concentrations of SiO_2 (27.97%), Fe_2O_3 (25.17%), CaO (2.66%) and low amounts of Al_2O_3 (0.54%), MgO (0.39%), TiO_2 (0.01%), K_2O (0.00%) and Na_2O (0.04%) (Table.2b).

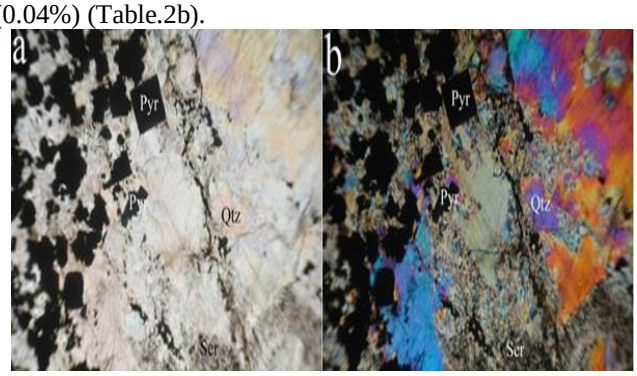

Fig.14 Photomicrograph of Copper ore shows cubic pyrite crystals in association with silver, quartz and sericite in (a) ppl, 4x and (b) xpl, 4x

k) PR-11. Dolerite: Plagioclase crystals are enclosed or partially wrapped by large crystals of pyroxene. These plagioclase exhibits ophitic to sub-ophitic texture with lath shaped structure. Clinopyroxene minerals are reacting with feldspar gives rise to orthopyroxene and Hypersthene (Hyp). Augite shows greenish blue color under crossed Nicol polarized light (XPL); while green to colorless under plane polarized light (PPL) with lath shaped and prismatic habit. Major minerals are Augite (Aug), Diopside (Diop) and Plagioclase (Plag) shows association with opaque iron oxides (Fe) (Fig.15).

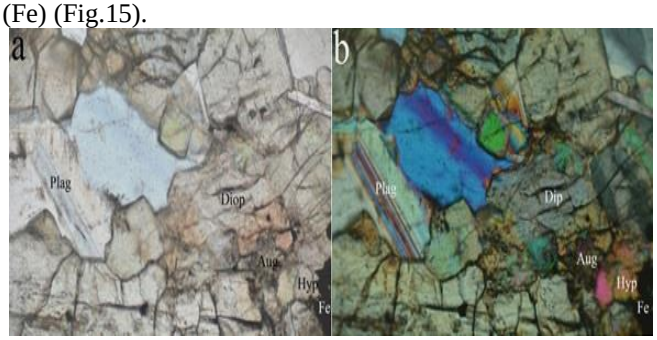

Fig.15 Photomicrograph of Dolerite shows ophitic to sub-ophitic texture of Plagioclase in (a) ppl, 4x and (b) xpl, 4x

l) PR-12. Auriferous quartzite: Quartz (Qtz) is anhedral, colourless and shows undulose extinction with minor Biotite (Bt) and Chlorite (Chl). Biotites are tabular with serrated margins, light brown in color, pleochroic from light brown to brown exhibiting straight extinction. Chlorite grains exhibit subhedral with pale green to light pale green pleochroism. Biotite is mostly altered to chlorite (Fig.16). The major element analysis of the rock samples showed high concentrations of SiO_2 (95.81%) and low amounts of Fe_2O_3 (1.79%), Al_2O_3 (0.75%), MgO (0.67%), TiO_2 (0.07%), K_2O (0.02%), Na_2O (0.04%) and CaO (0.03%) (Table.2b).

Fig.16 Photomicrograph of Auriferous quartzite containing biotite (Bt) and Chlorite (Chl) in (a) ppl, 4x and (b) xpl, 4x

m) PR-13. Quartz vein: Quartz (Qtz) grains show low relief, anhedral, indistinct cleavage and exhibit characteristic interference colors are seen in thin section. Plagioclase (Plag) exhibits ophitic to sub-ophitic texture with lath shaped structure. Bladed flakes of lithium-rich mica (lepidolite) minerals are observed in association with minor biotite (Bt) and pyrite. Biotites are tabular with serrated margins, light brown in color, pleochroic from light brown to brown exhibiting straight extinction (Fig.17). The major element analysis of the rock samples showed high concentrations of SiO_2 (98.97%) and low amounts of Fe_2O_3 (0.45%), Al_2O_3 (0.07%), MgO (0.17%), TiO_2 (0.01%), Na_2O (0.03%) and CaO (0.02%) (Table.2b).

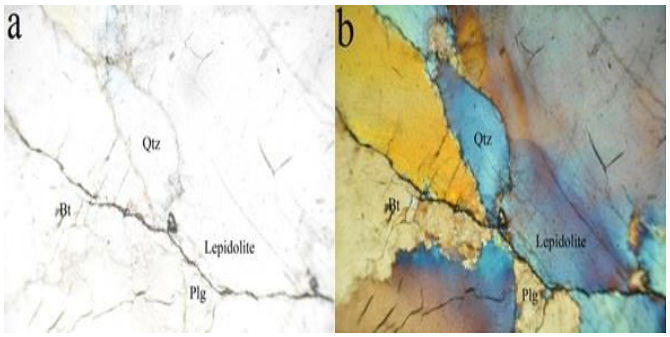

Fig.17 Photomicrograph of Quartz vein showing Lithium (Lepidolite-bluish pink color) mica in (a) ppl, 4x and (b) xpl, 4x

n) PR-14. Actinolite-Tremolite schist: Tremolite (Tre) shows grey colored, ladder shaped mineral is stretched due to deformation. Chlorite (Chl) appear as greenish groundmass exhibiting subhedral with pale green to light pale green pleochroism and shows association with acicular needles of green Actinolite (Act) mineral and minor opaque mineral Magnetite (Mag). Quartz (Qtz) grains show low relief, anhedral, indistinct cleavage and exhibit characteristic interference colors are seen in thin section (Fig.18).

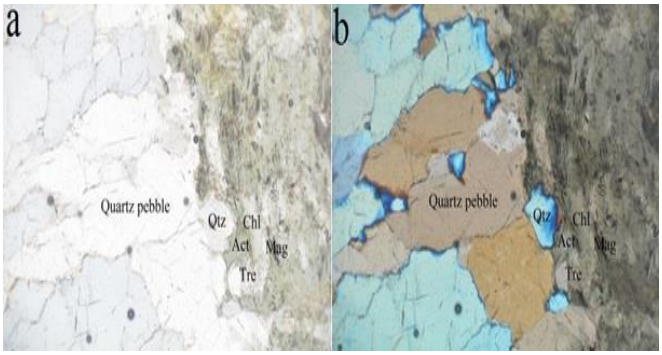

Fig.18 Photomicrograph of Actinolite-tremolite Schist showing deformed mineralized quartz pebbles in (a) ppl, 4x and (b) xpl, 4x

Table.2a Geochemical analysis data of the Major Elements from the study area (Except PR-5 & PR-8)

Elements (wt%)	Selected rock samples (PR-1 to PR-7)					
	PR-1	**PR-2**	**PR-3**	**PR-4**	**PR-6**	**PR-7**
SiO_2	25.49	42.17	6.38	40.37	77.91	65.89
Al_2O_3	3.37	0.30	0.21	3.24	9.92	10.11
BaO	-	0.78	0.00	-	-	-
TiO_2	0.11	0.11	0.01	0.22	0.39	1.23
Fe_2O_3	61.50	15.32	0.67	10.17	1.89	8.89
MnO	5.33	34.39	0.78	0.14	0.001	0.13
MgO	1.53	0.36	4.94	32.42	0.69	4.13
CaO	0.25	0.13	43.61	2.37	0.43	3.79
Na_2O	0.42	--	0.05	0.25	0.23	1.02
K_2O	0.23	0.11	0.05	0.10	5.18	3.29
P_2O_5	0.02	0.19	0.00	0.13	0.59	0.61
SO_3	n.d	n.d	0.03	n.d	n.d	n.d
H_20^+	-	4.93	42.19	8.72	0.43	-
Au (ppb)	n.d	--	<1	n.d	n.d	n.d
Ag (ppm)	n.d	<0.01	0.5	n.d	n.d	n.d
Cu (ppm)	n.d	<0.5	8	n.d	n.d	n.d
Zn (ppm)	n.d	--	<10	n.d	n.d	n.d
Li (ppm)	n.d	0.6	12.5	n.d	n.d	n.d
Pb (ppm)	n.d	0.2	24	n.d	n.d	n.d
Ni (ppm)	n.d	0.8	8	n.d	n.d	n.d
Co (ppm)	n.d	3	1.9	n.d	n.d	n.d
As (ppm)	n.d	1	1.8	n.d	n.d	n.d
Total	**98.25**	**98.79**	**98.92**	**98.13**	**97.66**	**99.09**
Rock type	**BHQ**	**Manganese**	**Dolo-limestone**	**Komatiites**	**Fuchsite quartzite**	**Talya Conglomerate**

Table.2b Geochemical analysis data of the Major Elements from the study area

Elements (wt%)	Selected rock samples (PR-9 to PR-14)				
	PR-9	**PR-10**	**PR-12**	**PR-13**	**PR-14**
SiO_2	49.90	27.97	95.81	98.97	62.24
Al_2O_3	13.89	0.54	0.75	0.07	9.06
BaO	-	0.00	0.00	0.00	0.01
TiO_2	1.09	0.01	0.07	0.01	2.29
Fe_2O_3	10.41	25.17	1.79	0.45	13.13
MnO	0.19	0.21	0.03	0.01	0.25
MgO	9.34	0.39	0.67	0.17	7.45
CaO	7.70	2.66	0.03	0.02	0.57
Na_2O	2.04	0.04	0.04	0.03	0.03
K_2O	0.69	0.00	0.02	0.00	0.06
P_2O_5	0.34	0.57	0.00	0.00	0.24
SO_3	n.d	33.94	0.02	0.01	0.03
H_20^+	2.96	8.40	0.61	0.13	4.50
Au (ppb)	n.d	***162***	3	<1	3
Ag (ppm)	n.d	***100.3***	<0.1	0.1	<0.1
Cu (ppm)	n.d	***160638***	11	5	2
Li (ppm)	n.d	0.0	7.0	7.8	22.4
Zn (ppm)	n.d	***10779***	25	<10	***204***
Pb (ppm)	n.d	***4075***	16	15	***684***
Ni (ppm)	n.d	89	39	11	***143***
Co (ppm)	n.d	***465.6***	5.3	1.2	***52.0***
As (ppm)	n.d	***644.1***	0.0	0.0	0.6
Total	**98.64**	**65.96**	**99.82**	**99.86**	**99.83**
Rock type	**Meta-gabbro**	**Copper ore**	**Auriferous Quartz**	**Quartz vein**	**Actinolite-Tremolite schist**

Note: n.d- not determined

The major element analysis of the rock samples showed high concentrations of SiO_2 (62.24%), Fe_2O_3 (13.13%), Al_2O_3 (9.06%), MgO (7.45%), TiO_2 (2.29%) and low amounts of K_2O (0.06%), Na_2O (0.03%) and CaO (0.57%) (Table.2b).

B. Spectral Signatures Study

Reflectance spectra of the 14 samples from the Precambrian basement (metavolcanic and metavolcano-sedimentary) in Chitradurga district of Dharwar Craton were measured in the Laboratory using the instrument ASD FieldSpec^3 which records 2151 channels with spectral range from 0.350 to 2.5 µm. These laboratory spectra's were measured with mean of each sixteen spectra (Ali M. Qaid., 2008). The massive exposures of the samples are found at the lower levels of the hill (Jayananda et al., 2008) have strong absorption in the ultraviolet blue wavelength region (0.45-0.52µm) and have high red reflectance in the wavelength of band of 0.63-0.69µm (Ali M. Qaid et al., 2009; Rajendran et al., 2011). The overtones of water could be seen in reflectance spectra of H_2O bearing minerals, the first overtone of the OH stretches occurs at about 1.4µm and the combinations of H-O-H band with the OH stretches are found near 1.9µm (Van der Meer and De Jong., 2001). A mineral whose spectrum has a 1.9µm absorption band contains water; but a spectrum that has feature absorption at 1.4µm and without absorption at 1.9µm band indicates the presence of hydroxyl. The combination metal -OH band stretch occurs near 2.2µm to 2.3µm and it is very typical diagnostic of mineralogy (Van der meer and De jong, 2001).

a) PR-1. Banded Hematite Quartzite (BHQ): The mean ASD spectral plot of sixteen spectra from four Banded Hematite Quartzite samples show absorption feature around 0.56µm and 1µm due to the presence of Fe^{3+} and Fe^{2+}. Iron oxides show strong absorption in the ultraviolet blue wavelength region (0.45-0.52µm) and high red reflectance in the range wavelength of band (0.63-0.69µm) (Ali M. Qaid et al., 2009) (Fig.19). Hematite shows intense absorption feature in 0.55µm of the electromagnetic spectrum (Hunt et al., 1971). Absorption anomalies at wavelength less than 0.9 µm is a good indicator and shows strong absorption representing hematite presence. Goethite shows absorption feature in the regions 0.55 µm and 0.9 µm of Fe^{3+} and Fe^{2+} ions respectively (Basavarajappa et al., 2015a). Existing ferric ion shows absorption features in the regions 0.5 µm and 0.9 µm with low reflectance in the VNIR region (Ali M. Qaid et al., 2009). The Siliceous minerals occur as quartz and feldspar produce very strong fundamental bands in the thermal infrared (TIR) region of 8-12 µm; but doesn't occur

in VNIR to SWIR regions (0.4 µm – 2.5 µm) of EM spectrum (Hunt., 1977; 1980).

b) PR-2. Manganeferous quartzite: The reflectance spectrum of Manganeferous quartzite depends on the presence of major minerals composition of its surface, mainly pyrolusite, psilomelane and weathering minerals (Rajendran et al., 2013). The manganese quartzite consist of pyrolusite (MnO_2) and manganite (MnO (OH)) show weaker absorption around 0.7 µm (Fig.19). The lab spectra of pyrolusite and manganite minerals shows spectrally featureless, quite low reflectance, strong absorption throughout the entire visible (0.3 - 0.7 µm) and reflective infrared (0.7 - 3 µm) spectral regions (Hunt and Salisbury, 1971; Hunt, 1977; Clark et al., 2003; Ibrahim et al., 2010) due to the presence of predominant Mn-O molecules. The Siliceous minerals occur as quartz and feldspar which but doesn't show any spectral absorption in VNIR to SWIR regions (0.4 µm – 2.5 µm) of EM spectrum (Hunt., 1977; 1980; Ali M. Qaid et al., 2009).

c) PR-3. Dolo-limestone: Many works have been carried out and reported on the application of Remote Sensing for Dolo-limestone mapping. It shows weaker absorption at 1.9 µm, 2.1 µm and 2.35 µm (Hunt, 1977; Clark., 1999; Gaffey., 1987). Gupta (2003), suggests various absorption regions of carbonate mineral in the shortwave infrared region such as 1.90 µm, 2.00 µm, 2.16 µm, 2.35 µm, 2.55 µm (Suranjith, 2012). The lab spectra of dolo-limestone absorptions are characteristically broad at 2.34 µm for calcite, but shifts to 2.51 µm and 2.319 µm due to substitution of Mg^{2+} for Ca^{2+} (Fig.19) (Rajendran and Sobhi Nasir., 2014). Carbonate absorption feature appeared at 2.35 µm; while Fe, Mg-OH is at 2.25 µm and 2.33 µm. The spectral curve of dolo-limestone is slightly affected due to the presence of epidote showing absorption nearly at 1.12 and 2.31 µm (Ali M. Qaid., 2008).

d) PR-4. Komatiites: Komatiites are mapped based on their spectral absorptions including the MgO-rich serpentines (Rajendran et al., 2012; Rowan et al., 2006; Ali M. Qaid et al., 2009). The study of minerals of phyllosilicates showed narrow spectral absorption features near 2.2 µm wavelength region due to mainly presence of A1-OH contents in the minerals. The octahedral sites in the phyllosilicates are occupied by magnesium instead of aluminum, the combination OH stretch produces (Mg-OH bending) strong absorption features in the vicinity of 2.30 to 2.35 µm (Hunt, 1977; Abrams et al., 1988; Mars and Rowan., 2010; Rajendran and Sobhi Nasir, 2014). In this study, the Mg-rich altered serpentine minerals are a key element to recognize komatiite (King and Clark., 1989). As well as, spectral absorptions of the OH and H_2O contents of the rocks and bearing minerals that are representing the metamorphic reaction with water within Archaean Komatiites, (Shrivastava et al., 2009). These can be interpreted in the near 1.39 to 1.90 µm respectively (Ali M. Qaid et al., 2009). The spectra of the komatiite samples shows well identified absorption features near 0.7, 0.9 to 1.10, 1.40, 2.30, 2.38 and 2.47 µm (Fig.19). In the spectra, the shallow absorptions near 0.7 µm and the broad deep absorptions from 0.9 to 1.10 µm are due to presence of ferrous iron content present on the surface of the samples. The sharp and deep absorption at 1.40 µm is due to presence of OH and H_2O contents present in the altered minerals of the samples. The significant absorption at 2.30 is due to the presence of Mg-OH and the shallow absorptions near 2.38 and 2.47 µm are influenced by the FeMg-OH contents in the samples (Ali M. Qaid., 2008).

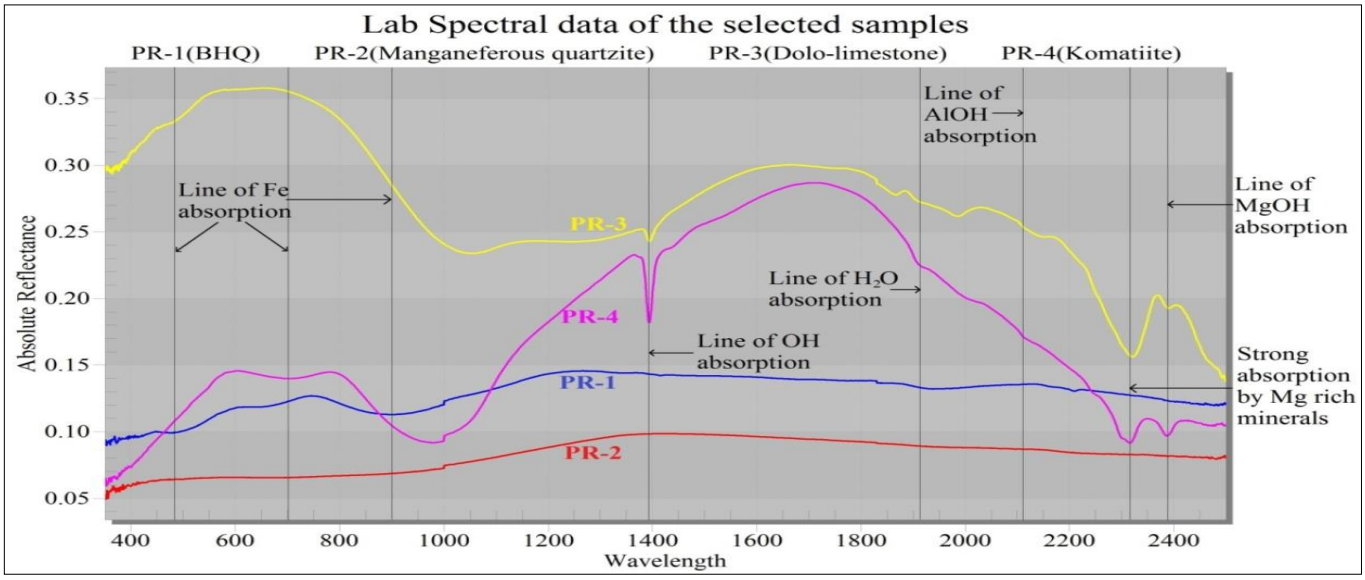

Fig.19 Lab Spectra of Banded Hematite Quartzite (PR-1); Manganeferous quartzite (PR-2); Dolo-limestone (PR-3); Komatiite (PR-4)

e) PR-5. Gneiss: Gneiss consists of plagioclase has absorption features around 1.4, and 2.2 µm; biotite has absorption features at 2.2 µm; muscovite has absorption features at 1.4, 1.9 and 2.2 µm and chlorite has absorption features at 2.25 µm (Fig.20). Quartz has absorption features at 2.15 µm due to water molecule inclusions. Muscovite is the dominant mineral with absorption features in the SWIR region (Ali M. Qaid., 2008).

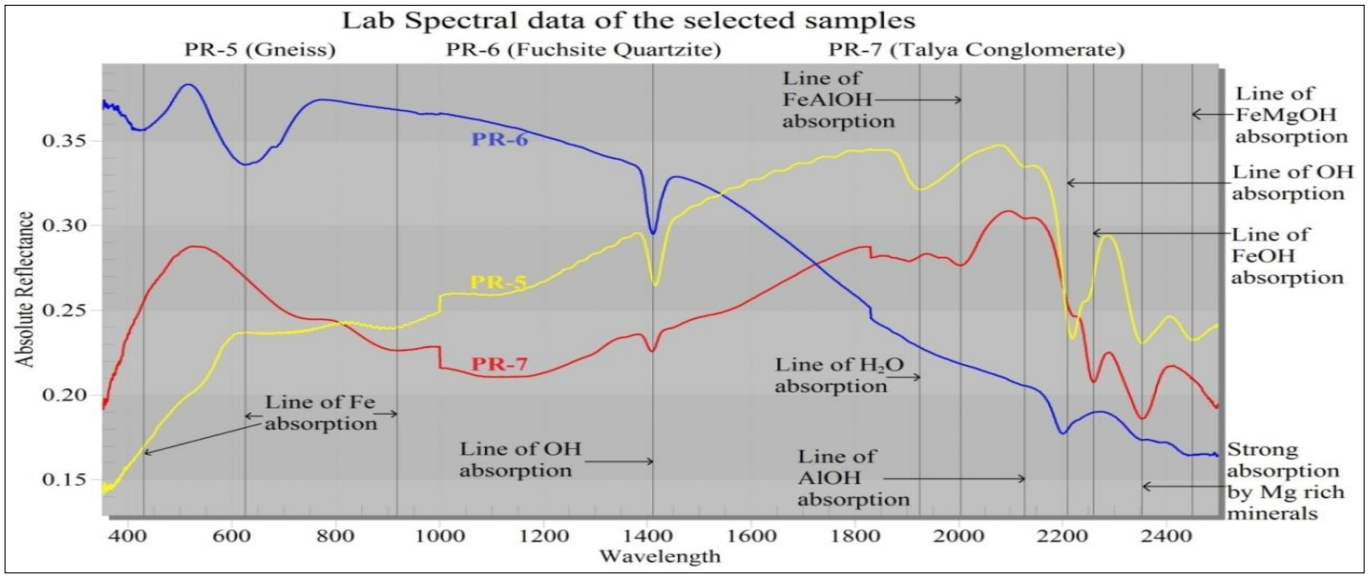

Fig.20: Lab Spectra of Gneiss (PR-5); Fuchsite Quartzite (PR-6); Talya Conglomerate (PR-7)

f) PR-6. Fuchsite quartzite: The silica minerals in Fuchsite quartzite do not cause spectral featuers in the VNIR to SWIR regions (0.4 µm – 2.5 µm) of EM spectrum (Hunt., 1977; 1980). The Si-O bonds produce very strong fundamental bands in the thermal infrared (TIR) reion of 8-12 µm (Hunt, 1980) (Fig.20). Quartz does not show any absorption features at 2.15 µm; while muscovite shows its absorption features around 1.4, 1.9 and 2.2 µm (Ali M. Qaid., 2008).

g) PR-7. Talya Conglomerate: The silica minerals in Talya Conglomerate do not cause spectral featuers in the VNIR to SWIR regions (0.4 µm – 2.5 µm) of EM spectrum (Hunt., 1977; 1980). The spectral curve exhibited absorption features of Fe, Mg-OH in 2.25 µm and 2.4 µm, which are characteristic of chlorite. The absorption feature 1 µm is characteristic Fe^{3+} ions. The lab spectral absorptions are characteristic at 2.34 µm for calcite; while 2.25 µm for Fe, Mg-OH and 2.35 µm due to strong absorption by carbonate minerals (Fig.20). Plagioclase shows its absorption around 1.4 and 2.2 µm; biotite has absorption features at 2.2 µm; muscovite has absorption features at 1.4, 1.9 and 2.2 µm. Actinolite is a fe rich mineral showing its absorption around 0.7, 0.9, 2.0 and 2.45 µm (Ali M. Qaid., 2008).

h) PR-8. Biotite Granite: Biotite Granite consists of plagioclase has absorption features around 1.4 and 2.2µm; biotite has absorption features at 2.2µm; muscovite has absorption features at 1.4, 1.9 and 2.2µm; chlorite has absorption features at 2.25µm & quartz has absorption features at 2.15µm due to the inclusions of water molecules (Fig.21). Muscovite is the dominant mineral with absorption features in the SWIR region. Sphene has quite low and weaker absorption from 0.9 to 2.5µm (Ali M. Qaid., 2008).

i) PR-9. Metagabbro: The laboratory spectral reflectance curves of Metagabbro show intense absorption features in the regions 1.4 µm (OH), 1.9 µm (H_2O) and 2.33 µm (Fe, Mg-OH). Fe^{3+} and Fe^{2+} displayed absorption features in 0.57 µm and 1 µm respectively. A gabbroic spectrum is characterized by two hydroxyl bonds centered on 2.26µm and 2.33µm. The weak to moderate absorption feature at 2.33µm is of Fe, Mg-OH feature and is related to biotite and/ or hornblende. Chlorite has its absorption around 2.25µm; while plagioclase has absorption features around 1.4, and 2.2µm. Hypersthene has its absorption around 1.4, 1.87 and 2.30µm; augite has at 2.27µm; diopside has at 2.37µm and pyroxene has at 2.38µm (Fig.21) (Ali M. Qaid., 2008).

j) PR-10. Ingaldhal Copper ore: The laboratory spectra curves of Copper ore collected from Ingaldhalu area exhibit similar spectral features of pyrite, arsenopyrite; but quartz do not exhibit any spectral features in the regions of VNIR and SWIR so that their existent in the rocks affect the general spectral features of other components (Fig.21). Pyrite shows its absorption at 1.15 and iron oxides around 0.87µm (Ali M. Qaid., 2008).

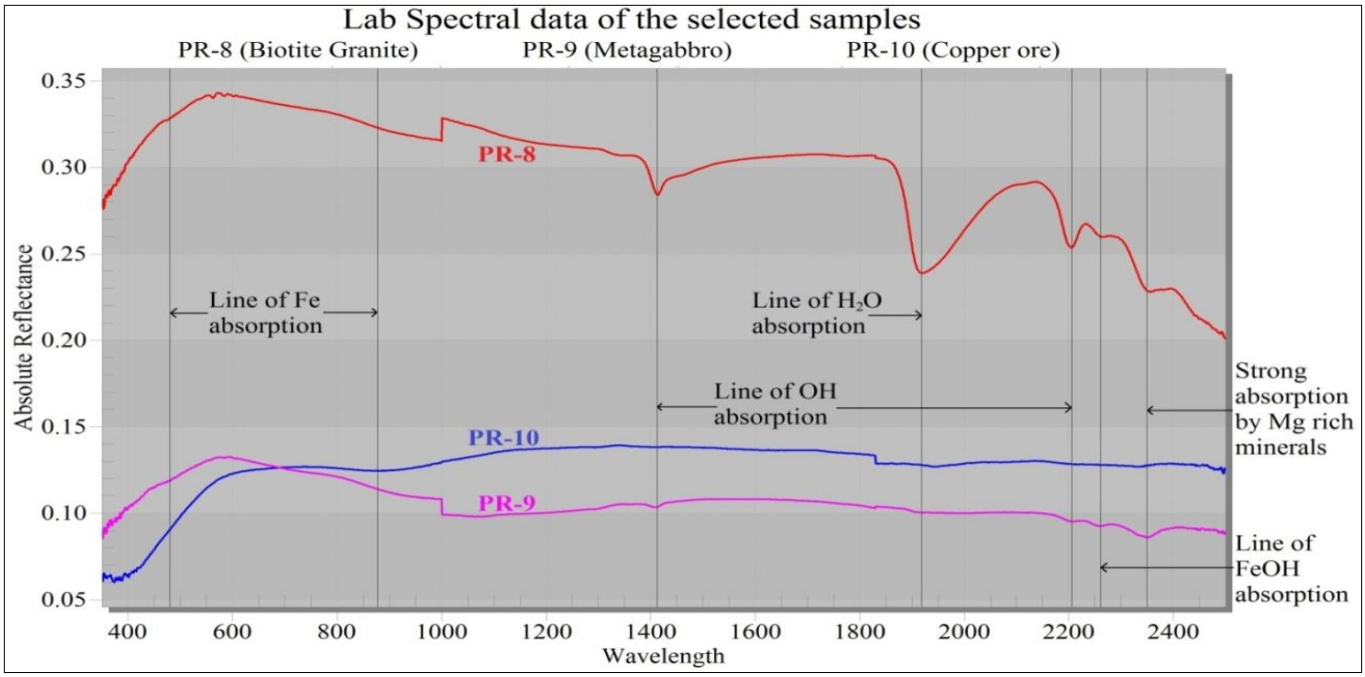

Fig.21 Lab Spectra of Biotite Granite (PR-8); Metagabbro (PR-9); Copper ore (PR-10)

k) PR-11. Dolerite: Dolerite consists of plagioclase has absorption features around 1.4, and 2.2µm. Hypersthene shows its absorption around 1.4, 1.87 and 2.30µm; augite shows at 2.27µm; diopside shows at 2.37µm and pyroxene shows at 2.38µm. Iron oxides has absorption around 0.47, 0.72 and 0.91µm (Fig.22).

l) PR-12. Auriferous quartzite: The silica minerals in auriferous quartzite do not cause spectral features in the VNIR to SWIR regions (0.4µm – 2.5µm) of EM spectrum (Hunt., 1977; 1980). The Si-O bonds produce very strong fundamental bands in the thermal infrared (TIR) region of 8-12µm (Hunt, 1980). Arsenopyrite and pyrite are clearly present, but they do not show any features in the spectral reflectance (Ali M. Qaid., 2008). Biotite has absorption features at 2.2µm; while chlorite has absorption features at 2.25µm (Fig.22).

m) PR-13. Quartz vein: The silica minerals in quartz vein do not cause spectral featuers in the VNIR to SWIR regions (0.4µm - 2.5µm) of EM spectrum (Hunt., 1977; 1980). The Si-O bonds produce very strong fundamental bands in the thermal infrared (TIR) region of 8-12µm (Hunt, 1980). Plagioclase has absorption features around 1.4 and 2.2µm; while biotite has absorption features at 2.2µm. The lithium rich lepidolite mica shows its absorption around 0.43, 0.56, 2.19, 2.34µm (Fig.22).

***n) PR-14. Actinolite-tremolite schist*:** The silica minerals in actinolite-tremolite schist do not cause spectral featuers in the VNIR to SWIR regions (0.4µm - 2.5µm) of EM spectrum (Hunt., 1977; 1980). The spectral curve exhibited absorption features of Fe, Mg-OH in 2.25µm and 2.4µm, which are characteristic of chlorite. Actinolite is a fe rich mineral showing its absorption around 0.7, 0.9, 2.0 and 2.45µm; while tremolite is a mg rich mineral showing its absorption around 2.36 and 2.39µm (Fig.22).

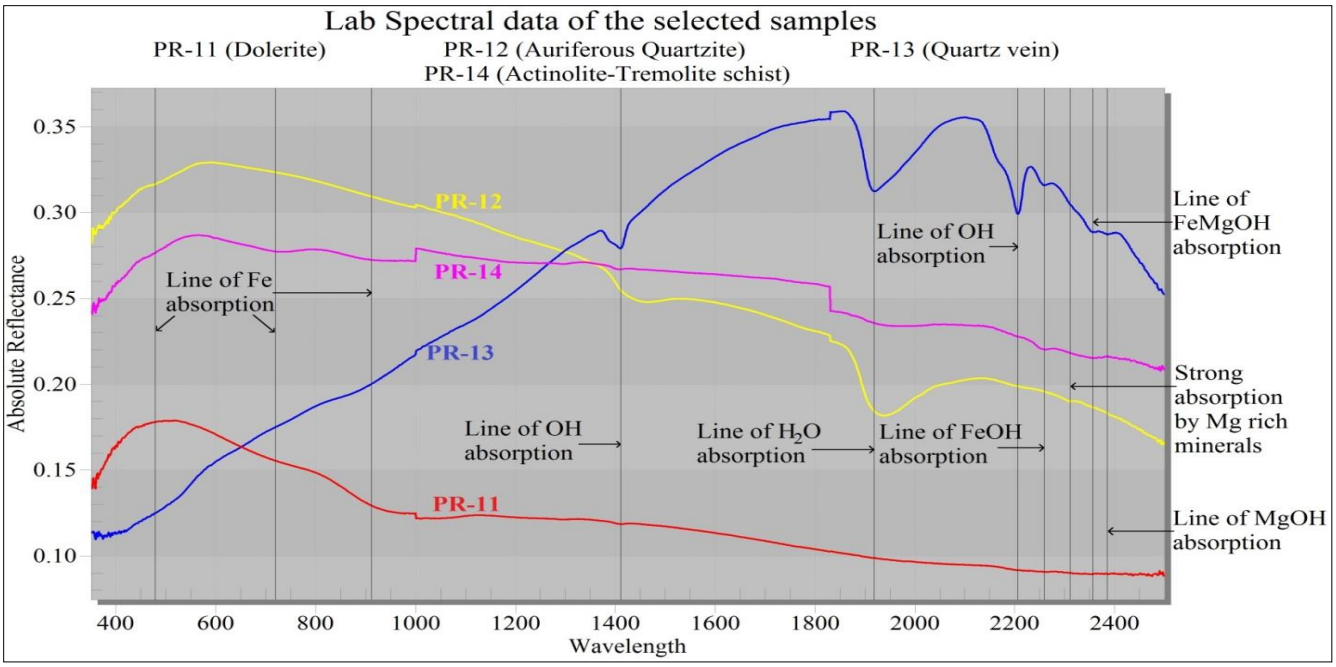

Fig.22 Lab Spectra of Dolerite (PR-11); Auriferous Quartzite (PR-12); Quartz vein (PR-13); Actinolite-Tremolite Schist (PR-14)

IV. DISCUSSION

A standard had generated further to prepare Indian spectral library of the selected samples of Chitradurga Schist Belt (CSB) through its petrological studies, geochemical and lab spectral signatures (Basavarajappa et al., 2015a) (Table.3). In future, this will help in generating our own Spectral Library for Indian Precambrian rocks by referring the Standard Spectral curves of specific minerals available in the USGS, JPL and JHU spectral library in Envi software (Rajendran et al., 2011). The absorption and reflection features are studied as described by Hunt and Salisbury (1970), Hunt et al., (1971), Hunt and Ashley (1979) and Blom et al., (1980) (Basavarajappa et al, 2017b). The fresh or weathered surface of iron metallic elements causes strong absorptions in Visible and Near Infrared region (Ali M. Qaid et al., 2009). Diagnositic absorption features of H_2O, OH, Al-OH, Mg-FeOH, CO_3 and FeOH in the regions of VNIR and SWIR of EM spectrum studied and revealed that the effect of mineralized zones, sericitification, oxidation, carbonatization, serpentinization and clay minerals.

The study shows that the spectral absorptions features depend on the mineral constituents and major elemental composition of the samples. Mafic rocks contain iron oxides, pyroxenes, amphiboles and magnetite and therefore absorption bands corresponding to ferrous and ferric iron appear at 0.7µm and 1.0µm respectively (Gupta, 2003). The spectral features of ultramafic rocks are dominated by the absorption of Fe, Mg-OH at 2.32µm, 2.38µm which is due to the presence of phlagophite, biotite and hornblende. Limestone and calcareous rocks exhibit absorption range at 1.9µm and 2.35µm respectively, ferrous ions exhibits spectral feature at 1.0µm which is more common in dolomites due to the substitution of Mg^{2+} by Fe^{2+} (Rajesh., 2004).

The petrological study showed the minerals of the rock and chemical analyses produced the concentration of chemical elements are characteristic features to the spectral absorptions at 1.4µm, 1.9µm and 2.31µm. Silicification is indistinguishable in the regions of VNIR and SWIR of the EM spectrum due to lack of diagnostic spectral absorption features in silica in this wavelength. The arsenopyrite and pyrite are not appear any absorption features in the range of spectra due to the exhibit trans-opaque behavior and often lack distinction in VNIR and SWIR. This study clearly demonstrated and documented the spectral absorption features of the selected rock samples in the study area mainly depend on the optical and physico-chemical characters of the rock.

The mineralized zones are concentrated in mainly in quartz vein intrusions and spread along the shear zones. The results of the chemical analyses revealed high anomalies of potential economic minerals and oxides like Au (162ppb), Ag (100.3ppm), Cu (160638ppm), Zn (10779ppm), Pb (4075ppm), Ni (143ppm), Li (22.4ppm), Co (465.6ppm), SO_3 (33.94%) and As (644.1ppm). The highest anomalies of gold are associated with the concentration of disseminated arsenopyrite and pyrite concentrated where the quartz veins are abundant and spread along the shear zones.

Table.3 Comprehensive model through the Integration of Hyperspectral and Geochemical Signatures study (Swaminath and Ramakrishnan, 1981)

		Major litho units of the study area		Minerals observed	Geochemistry (%)	Spectral range
DHARWAR SUPER GROUP	CHITRADURGA GROUP	Gabbro		Pyroxene	98.64	2.32 µm
				Augite		1.0, 2.21, 2.32 µm
				Diopside		1.07, 1.30, 2.32 µm
				Hypersthene		0.94, 1.87 µm
		Dolerite		Augite	--	1.05, 2.20, 2.32 µm
				Diopside		0.64, 1.05, 2.32 & 2.38 µm
				Hematite		0.52, 0.87, 1.89
				Hypersthene		0.91, 1.92 µm
		Younger granites		Biotite	--	0.87, 2.35 & 2.44 µm
				Chlorite		1.32, 1.92, 2.21, 2.26, 2.35, 2.44 µm
				Muscovite		0.87, 1.42, 1.92, 2.12, 2.21, 2.35, 2.44 µm
		Hiriyur Formation	BHQ	Hematite	53.50	0.48, 0.63, 0.87, 1.93,
		Ingaldhal Formation	Dolo-limestone	Calcite	47.61	1.86, 1.98, 2.31 µm
				Epidote		0.48, 1.12, 1.40, 1.86, 2.31 µm
		Vanivilas Formation	Talya conglomerate	Chlorite	99.09	1.35, 2.13, 2.26, 2.35, 2.47 µm
				Actinolite		0.63, 1.41, 2.13, 2.35 µm
				Biotite		0.63, 0.9, 2.35 & 2.47 µm
				Muscovite		0.63, 0.9, 1.41, 1.95, 2.13, 2.22, 2.35, 2.47 µm
			Manganese	Pyrolusite	34.39	0.63-0.79, 0.93-1.11 µm
				Manganite		
	BABABUDAN GROUP	Serpentinite		Serpentine	32.42	2.32, 2.39 µm
				Olivine		0.7, 0.96, 1.91, 2.47 µm
				OH	8.72	1.40 µm
				H_2O		1.91, 2.21 µm
		Oligomictic conglomerate		--	--	--
PGC		Peninsular Gneissic Complex		Biotite	--	0.63, 0.9, 2.35 & 2.45 µm
				Muscovite	--	0.7, 0.9, 1.41, 1.92, 2.12, 2.21 µm
				Chlorite	--	1.4, 2.12, 2.21, 2.35, 2.45 µm
SARGUR		Fuchsite quartzite		Muscovite	--	0.63, 0.97, 1.41, 1.90, 2.21, 2.35, 2.44 µm
				Hematite	1.89	0.43, 0.63, 0.97 µm

V. CONCLUSION

The study of laboratory spectra and major elements distribution of selected samples provides basic information on the absorption characters of the major elements which may use for mapping of such Precambrian economic deposits. The spectral signatures of collected using ASD Spectro-radiometer in the wavelength range of 350-2500 nm showed the absorption characters of different economic minerals of the study area. The comparative analysis of spectral signatures of samples with the existing mineral spectral library shows best suitable spectral curves and these may be considered for mapping such economic minerals resources. Understanding of spectral absorption features of these rocks based on their optical and physico-chemical characters is significant in Remote Sensing technique to map the rock and explore the economic important minerals of the rock.

CONFLICTS OF INTEREST: The authors declare no conflicts of interest.

ACKNOWLEDGMENT

The authors are indepthly thank Prof. P.Madesh, Chairman, Department of Studies in Earth Science, Centre for Advanced Studies in Precambrian Geology, University of Mysore, Mysuru; Prof. Y.T. Krishne Gowda, Principal, Maharaja Institute of Technology Thandavapura, Mysuru. We are thankful to Dr. K.V. Krishnamurthy; Farmer Deputy Director; Ms. Nisha Rani; Mr. Sumit Kumar Ahirwar and Mr. Chethan Kashyap, for their valuable suggestions and assistance to this study. Geological Survey of

India, Bangalore is thanked for permission and measuring spectral data. This study is supported by the UGC-MRP grant (F No.42.73 (SR)/2012- 13, dt: 12.03.2012).

REFERENCE

[1] Abrams M.J, Rothery D.A, Pontual A,. Mapping in the Oman ophiolite using enhanced Landsat Thematic Mapper images, Tectonophysics, 151 (1988) 387-401.

[2] Ali Mohammed Qaid Saeed. Application of Remote Sensing and GIS techniques in Mapping of Hydrothermal alteration zones in North East of Hajjah, Yemen, Unpub Thesis, Univ. of Mysore, Mysuru, (2008) 1-237.

[3] Ali M Qaid Saeed, H.T. Basavarajappa and S. Rajendran. Integration of VNIR and SWIR Spectral Reflectance for Mapping Mineral Resources; A case study, North East of Hajjah, Yemen, J.Indian.Soc. Remote Sens, 37 (2009) 305-315.

[4] Basavarajappa H.T, Manjunatha M.C and Jeevan L. Application of geoinformatics on delineation of groundwater potential zones of Chitradurga district, Karnataka, India, International Journal of Computer Engineering and Technology, 5(5) (2014) 94-108.

[5] Basavarajappa H.T and Manjunatha M.C. Geoinformatic techniques on mapping and reclamation of wastelands in Chitradurga district, Karnataka, India, International Journal of Computer Engineering and Technology, 5(7) (2014) 99-110.

[6] Basavarajappa H.T, Manjunatha M.C and Rajendran S. Integration of Hyperspectral signatures and major elements of iron ore deposits around Holalkere range of Megalahalli, Chitradurga Schist Belt, Karnataka, India, Journal of The Indian Mineralogist, 49(1) (2015) 85-93.

[7] Basavarajappa H.T, Jeevan L, Rajendran S and Manjunatha M.C. Discrimination of Banded Magnetite Quartzite (BMQ) deposits and associated lithology of parts of Chikkanayakanahalli Schist Belt of Dharwar Craton, Karnataka, India using Remote Sensing Technique, International Journal of Advanced Remote Sensing and GIS, 4(1) (2015) 1033-1044.

[8] Basavarajappa H.T and Manjunatha M.C. Groundwater quality analysis in Precambrian rocks of Chitradurga district, Karnataka, India using geoinformatics technique, International conference on water resources, coastal and ocean engineering, Elsevier, Aquatic Procedia, 4 (2015) 1354-1365.

[9] Basavarajappa H.T, Maruthi N.E, Jeevan L and Manjunatha M.C. Physico-chemical characteristics and hyperspectral signature study using geomatics on gem variety of Corundum bearing Precambrian litho-units of Mavinahalli area, Mysuru district, Karnataka, India, International Journal of Computer Engineering & Technology, 9(1) (2016) 102-112.

[10] Basavarajappa H.T, Manjunatha M.C, Rajendran S and Jeevan L. Determination of Spectral characteristics on Archaean Komatiites in Ghattihosahalli Schist Belt (GSB) of Kumminagatta, Chitradurga district, Karnataka, India, International Journal of Advanced Remote Sensing and GIS, 6(1) (2017) 2416-2423.

[11] Basavarajappa H.T, Maruthi N.E and Manjunatha M.C. Hyperspectral signatures and field petrography of Corundum bearing litho-units in Arsikere band of Haranahalli, Hassan district, Karnataka, India, International Journal of Creative Research Thoughts, 5(4) (2017) 3791-3798.

[12] Basavarajappa H.T, Jeevan L, Rajendran S and Manjunatha M.C. ASTER mapping of Limestone deposits and associated lithounits of parts of Chikkanayakanahalli, Southern parts of Chitradurga Schist Belt, Dharwar Craton, India, Journal of the Indian Society of Remote Sensing, 47 (2019) 693-703.

[13] Blom R.G, Abrams M.J and Adams H.G. Spectral reflectance and discrimination of plutonic rocks in the 0.45–2.45μm region. J. Geophys. Res, 85 (1980) 2638–2648.

[14] CGWB. Central Ground Water Board, Groundwater Information Booklet, Chitradurga district, Karnataka, South Western region, Govt. of India, Bengaluru (2013) 1-31.

[15] Clark R.N, King T.V.V, Klejwa M and Swayze G.A. High spectral resolution spectroscopy of minerals, J.Geophys.Res, 95(B8) (1990) 12653-12680.

[16] Clark R.N. Spectroscopy of rocks and minerals and principles of spectroscopy. In Remote Sensing for the Earth Sciences, Edited by Rencz A.N and Ryerson R.R., John Wiley, New York, 3 (1999) 3-58.

[17] Clark R.N, Swayze G.A, Wise R, Livo K.E, Hoefen T.M, Kokaly R.F, Sutley S.J,. USGS Digital Spectral Library splib05a. U.S. Geological Survey, Open File Report: (2003) 03-395.

[18] Deshmuk S.D, Hari K.R, Diwan P and Basavarajappa H.T. Spinifex textured metabasalt of Sonakhan Greenstone Belt, Central India, Journal of The Indian Mineralogist, 42(1) (2008) 71-83.

[19] DID (2006). Detailed Information Dossier on Iron Ores in India, Geological Survey of India, Govt. of India, October: 1-194.

[20] ENVI. (2009). Atmospheric Correction Module: QUAC and FLAASH User's Guide.http://www.exelisvis.com/portals/0/ pdfs/envi/Flaash_Module.pdf2009.

[21] Gaffey S.J. Spectral reflectance of carbonate minerals in the visible and near infrared (0.35-2.55 micrometers): Anhydrous minerals, Journal of Geophysical Research, 92 (1987) 1429-1440.

[22] GSI. Geological Survey of India, Geology and Mineral Resources of the States of India, Part-VII, Karnataka & Goa, Miscellaneous Publication No.30, Govt. of India, Bangalore: (2006) 1-65.

[23] Gupta R.P (2003). Remote Sensing Geology, Springer.

[24] Hoover D.B, Heran W.D and Hill P.L. The Geophysical Expression of selected Mineral Deposit Models, United States, Department of the Interior Geological Survey: (1993) 58-60.

[25] Hunt G.R and Salisbury J.W,. Visible and near-infrared spectra of minerals and rocks, Modern Geology, 1 (1970) 283-300.

[26] Hunt G.R and Ashley R.P. Spectra of altered rocks in the visible and near infrared, Economic Geology, 74 (1979) 1613-1629.

[27] Hunt G.R, Salisbury J.W and Lehnoff C.J (1971). Visible and Near Infrared Spectra of Minerals and Rocks: III. Oxides and Oxy-hydroxides, Modern Geology (2) (1971)195-205.

[28] Hunt G.R. Spectral signatures of particular minerals in the visible and near infrared, Geophysics, 42 (1977) 501-513.

[29] Hunt G.R. Electromagnetic radiation: The communication link in remote sensing. In: B.S. Siegal and A.R. Gillespie, (Editors), Remote Sensing geology, John Wiley and Sons, New York: (1980) 5-46.

[30] Ibrahim, A., Salem Mohamed E. Ibrahim., Mohamed Abd El Monsef.,. Mineralogy, geochemistry, and origin of hydrothermal manganese veins at Wadi Maliek, Southern Eastern Desert, Egypt. Arab J Geosci. (2010) DOI 10.1007/s12517-010-0195-1.

[31] Jayananda M, Kano T, Peucat J.J and Channabasappa S. 3.35Ga Komatiite volcanism in the Western Dharwar Craton, Southern India: Constraints from Nd isotopes and whole-rock geochemistry, Elsevier, Science Direct, Precambrian Research, 162 (2008) 160-179.

[32] King T.V.V and Clark R.N.. Spectral characteristics of serpentines and chlorites using high resolution reflectance spectroscopy: Journal of Geophysical Research, 94 (1989) 13997-14008.

[33] Lipton G. Spectral and Microwave Remote Sensing: An Evolution from small scale regional studies on Mineral mapping and ore deposit targeting, Proceedings of Exploration-97, 4th Decennial International conference on Mineral exploration, Geomatics International Inc., Burlington, Canada: (1997) 43-58.

[34] Maclaren J. M. On some auriferous tracts in Southern India, Rec., Geol.Surv. India, 34(2) (1906) 45-136.

[35] Manjunatha M.C, Basavarajappa H.T and Jeevan L. Geomatics analysis on land use land cover classification system in Precambrian terrain of Chitradurga district, Karnataka, India, International Journal of Civil Engineering and Technology, 6(2) (2015) 46-60.

[36] Manjunatha M.C and Basavarajappa H.T. Spatial data integration of lithology, geomorphology and its impact on groundwater prospect zones in Precambrian terrain of Chitradurga district, Karnataka, India using geomatics application, Global Journal of Engineering Science and Research Management, 2(8) (2015) 16-22.

[37] Manjunatha M.C and Basavarajappa H.T. Spatio-temporal variation in Groundwater quality analysis on Chitradurga district, Karnataka, India using Geo-informatics technique, Journal of International Academic Research for Multidisciplinary, 3(11) (2015) 164-179.

[38] Manjunatha M.C, Basavarajappa H.T and Maruthi N.E. Land use/land cover change detection analysis in Holalkere taluk of Chitradurga district, Karnataka, India using Geoinformatics, Journal of

Environmental Science, Computer Science and Engineering & Technology, 6(3) (2017) 291-301.

[39] Manjunatha M.C. Applications of Hyperspectral Remote Sensing and GIS on NE-SW transects of Chitradurga district, Karnataka, India, Unpub Thesis, University of Mysore: (2017) 1-204.

[40] Manjunatha M.C and Basavarajappa H.T. Antropogenic pressure on forest cover and its change detection analysis using geoinformatics in Holalkere taluk of Chitradurga district, Karnataka, India, International Journal of Scientific Research in Science and Technology, 3(1) (2017) 71-76.

[41] Manjunatha M.C, Maruthi N.E, Siddaraju M.S and Basavarajappa H.T. Temporal mapping of forest resources in Hosadurga taluk of Karnataka state, India using geo-informatics, Journal of Emerging Technologies and Innovative Research, 5(11) (2018) 124-132.

[42] Manjunatha M.C and Basavarajappa H.T. Mapping of land units and its change detection analysis in Chitradurga taluk of Karnataka state, India using geospatial technology, International Advanced Research Journal in Science, Engineering and Technology, 7(7) (2020) 61-68.

[43] Manjunatha M.C and Basavarajappa H.T. ASTER spectral reflectance for lithological discrimination in Central parts of Chitradurga Schist Belt (CSB), Karnataka, India, International Journal of Geology and Mining, 7(1) (2021) 356-366.

[44] Mars J.C and Rowan L.C.,. Spectral assessment of new ASTER SWIR surface reflectance data products for spectroscopic mapping of rocks and minerals, Remote Sens. Environ, 114 (2010) 2011-2025.

[45] MRI, (xx). Mineral Resources of India, Geology and Mineral Resources of India, Govt. of India: 1-75.http://eptrienvis. nic.in/All%20PDF%20Files/Mineral%20Resources%20of%20India.pdf

[46] Nisha Rani, Summit Kumar Ahirwar and Jamalanwar. Hyperspectral Remote Sensing Studies of Mafic-Ultramafic rocks of Sargur and Bababudan Groups, Hassan district, Karnataka, South India, Journal of The Indian Mineralogist, 48(2) (2014) 239-248.

[47] Prabhakar B.C and Namratha R. Morphology and textures of Komatiite flows of J.C Pura Schist Belt, Dharwar Craton, Journal of Geological Society of India, 83 (2014) 13-20.

[48] Radhakrishna B.P and Sreenivasaiah G. Bedded barite from the Precambrian of Karnataka, J.Geol.Soc.India, 15 (1974) 314-315.

[49] Rajendran, S. and Sobhi Nasir. Hydrothermal Altered Serpentinized Zone and a Study of Ni-Magnesioferrite – Magnetite - Awaruite Occurrences in Wadi Hibi, Northern Oman Mountain: Discrimination through ASTER Mapping, Ore Geology Reviews, 62 (2014) 211-226.

[50] Rajendran, S., Thirunavukkarasu, A., Balamurugan, G. and Shankar, K.. Discrimination of Iron Ore Deposits of Granulite Terrain of Southern Peninsular India using ASTER Data. Journal of Asian Earth Sciences, 41 (2011) 99-106.

[51] Rajendran, S., Salah al-Khirbash, Bernhard Pracejus, Sobhi Nasir, Amani Humaid Al-Abri, Timothy M. Kusky and Abuduwasit Ghulam. ASTER Detection of Chromite Bearing Mineralized Zones in Semail Ophiolite Massifs of the northern Oman Mountain. Exploration Strategy, Ore Geology Reviews, 44 (2012) 121-135.

[52] Rajendran, S and Nasir, S. ASTER spectral analysis of ultramafic lamprophyres (carbonatites and aillikites) within the Batain nappe, northeastern margin of Oman-a proposal developed for spectral absorption. Int. J. Remote Sens. 34(8) (2013) 2763-2795.

[53] Rajesh H.M. Application of Remote Sensing and GIS in Mineral Resource Mapping-An Overview, J. Miner. Petrol.Sci, 99(3) (2004) 83-103.

[54] Ramachandran T.V and Ramanamurthy M.V. Utility of a low cost, India-designed Spectro-radiometer in ground reflectance studies-a case study from Chitradurga area, Karnataka state, GSI Rec. 113 (1982) 115-119.

[55] Ramakrishnan M, Mahabaleswar B and Viswanathan S. The abundances of some Trace-elements in the First-ever Reported Sample of Spinifex-Textured Komatiite from Ghattihosahalli, Karnataka, Jour. Geol.Soc.Ind., 79 (2012) 361-366.

[56] Ravikumar P, Deljo Davis, Sharika Mathew, Somashekar R.K and Prakash K.L., Spatio-temporal variation in random concentration in groundwater with respect to rock types: A case study from Chitradurga district, Karnataka, Journal of Geological Society of India, 83 (2014) 156-164.

[57] Rowan L.C, Schmidt R.G and Mars J.C., Distribution of hydrothermally altered rocks in the Reko Diq, Pakistan, Remote Sensing of Environment, 104 (2006) 74-87.

[58] Seshadri T.S, Chaudhuri A, Harinadha Babu P and Chayapathi N. Chitradurga Belt, Early Precambrian Supracrustals of Southern Karnataka, Editors: Swami Nath J and Ramakrishnan M, Memoirs of the Geological Survey of India, 112 (1981) 163-198.

[59] Shrivastava K.L, Anju Mathur and Mamta Chauhan., Recent Advances in the Understanding of Komatiites with special reference to Ore Genesis., Earth System Sciences, Felicitation Volumes in Honour of Prof. V.K. Verma, Concept Publishing Company, New Delhi, 1 (2009) 295-323.

[60] Suranjith K.J. Hyperspectral and Multispectral approaches for Exploration and characterization of certain deposits of Bauxite, iron ore and limestone in South India, (2012) Unpub PhD thesis, Department of Geology, Anna University, Chennai.

[61] Swaminath J and Ramakrishnan M. Early Precambrian Supracrustals of Southern Karnataka, A Geological Survey of India, Govt. of India, 112 (1981) 163-198.

[62] Thutupalli G.K.M, Lu G.V, Nevada K.C, Krishnanunni K, Ramachandran T.V and Ramanamurthy M.V. Application of an indigeneously designed spectro-radiometer in ground truth collection, Remote Sensing in subsurface exploration, AEG (Proceedings of the Colloquium on Remote Sensing, AEG Seminar): (1981) 143-151.

[63] Van der Meer F.D and De Jong (Eds), S.M. Basic principles and prospective applications, book series remote sensing and digital image processing, Kluwer Academic publishers, Dordrecht: (2001) 403.

[64] Vishwanatha M.N, Ramakrishnan M and Narayana Kutty T.R., Possible spinifex texture in a serpentinite from Karnataka, J. Geol. Soc. India, 18 (1977) 194-197.

[65] Viswanathaiah M.N and Venkatachalapathi V. Microbiota from the Bababudan iron formation, Karnataka, J.Geol.Soc.India, 21 (1980) 16-20.